Submitted to *J. Geophys. Res.*, 23 March, 2001. 1st revision 17 July, 2001. 3rd revision 15 Dec, 2001.

Global IMAGE/HENA observations of the ring current: Examples of rapid response to IMF and ring current-plasmasphere interaction

P. C:son Brandt[1], D. G. Mitchell[1], Y. Ebihara[2], B. R. Sandel[3], E. C. Roelof[1], J. L. Burch[4], R. Demajistre[1]

Abstract. Energetic neutral atom (ENA) images in the energy range 16-50 keV obtained by the ENA imager HENA onboard the IMAGE satellite are presented from the period 23-26 May 2000. Two events during this period are investigated: (1) A rapid decrease on 23 May of the entire dayside ring current ¤uxes; (2) An unexpected local time distribution of the ring current during the storm commencing on 24 May. In the £rst event, ENA ¤uxes from the dayside ring current decrease rapidly during 10 min. The start of the decrease is associated with a sharp, southward turning of the interplanetary magnetic £eld (IMF) and a steep increase of the cross polar cap potential (PCP). Simulated equatorial ion ¤uxes are able to reproduce the event using a kinetic ion drift model. The observations are explained in terms of rapidly changing drift paths during a recon£guration of the convectional electric £eld in the magnetosphere. The recon£guration timescale ($\sim$10 min) is too short to modify the pitch angle distribution (PAD). The results show that the solar wind electric £eld over the dayside magnetosphere penetrates to the inner magnetosphere within a few minutes. In the second event, an enhanced ring current during the storm on the 24 May develops. Below 27 keV at L$<$4 the ring current extends from midnight clockwise through noon towards the dawn sector. At energies above 27 keV the images show an enhancement in the ENA emissions coming from the noon region and a lack of ENA emissions from the duskside. Apart from the main phase of the storm, the convection through the magnetosphere was steady throughout the three-day recovery phase. Images in extreme ultraviolet (EUV) of the plasmasphere reveal a spatial relation between the ENA emissions and a plasmaspheric tail. Data from the Polar satellite together with preliminary ENA simulations suggest that the lack of ENA emissions is an effect of ion PADs peaked around 90°. We discuss possible explanations for the modi£cation of the PADs, such as adiabatic drifts, charge exchange, and wave-particle interaction.

1. Introduction

Energetic neutral atoms (ENA) are produced when singly positively charged energetic ions undergo charge-exchange collisions with cold neutral atoms or molecules. The ions will become neutral and propagate unaffected by electromagnetic £elds. If the initial energy is much greater than the planetary escape energy (0.6 eV/nucleon), then the ENA are unaffected by gravitational £elds and will maintain their energy and momentum. In the terrestrial magnetosphere, the ring current will charge exchange with the geocorona at high altitudes and emit ENAs. In this way the ring current plasma can be imaged. In addition to carrying with it spectral and directional information of the energetic ions, the ENA also

[1]Applied Physics Laboratory, Laurel, Maryland
[2]National Institute of Polar Research, Tokyo, Japan
[3]University of Arizona, Tucson, Arizona
[4]Southwest Research Institute, San Antonio, Texas

is a direct measurement of the composition of those ions.

ENA imaging was £rst conceptualized by *Roelof et al.* [1985] and has today become an important tool for space plasma diagnostics. ENA images of the ring current have been obtained from several spacecrafts [*Roelof*, 1987; *Henderson et al.*, 1997] using charged particle telescopes in the polar regions of the magnetosphere devoid of charged particles where the detectors therefore responded mainly to the weak ENA emissions. Dedicated ENA imagers have been carried by the Astrid satellite [*Barabash*, 1995; *C:son Brandt et al.*, 1999], Cassini [*Mitchell et al.*, 1998] and now IMAGE [*Mitchell et al.*, 2000].

IMAGE was launched in March 2000 into a polar, elliptical orbit with an apogee altitude of 7.2 Earth radii (R_E) (45,922 km/28,472 mi) [*Burch*, 2000]. The location of the apogee will change during the course of the two-year mission, both in latitude and in local time. At the beginning of the mission, apogee was at approximately 40°north latitude and at dusk local time. As the Earth moves around the Sun, the plane of the orbit will shift relative to the Earth-Sun line (by 30°longitude per month). For the data reported in this paper the orbit plane was approximately along the 1400-0200 magnetic local time (MLT) meridian and the magnetic latitude of apogee was about 50°on the dayside.

In this paper we will present the initial analysis of two opposing events takning place in the period 23-26 May, 2000. On the 23 May HENA observed an enhancement of the dayside ring current ¤ux near L=4. Within less than 10 min the entire dayside ENA ¤ux decreased by roughly four times. This sudden decrease in ENA ¤ux occured when a relatively high northward IMF quickly turned southward.

The second event takes place on 24 May when HENA observed an unexpected behavior of the development of the storm. The ENA emissions above 27 keV from the ring current varied greatly with local time with the maximum intensity around noon in the early stages of the storm. In the later stages of the storm, the maximum intensity was found on the duskside, but appeared on the noon side again in the late recovery phase. However, the local time pattern always appeared closely related to the location and shape of the plasmapause and the plasmaspheric tail [*Grebowsky*, 1970].

In the following sections we will describe the £rst event on 23 May, 2000 and use the ring current model by *Ebihara and Ejiri* [2000] to give a preliminary explanation in terms of rapidly changing drift paths due to changing convectional electric £eld. Second, we will present ENA images from different phases of the storm and describe their relation to data from POLAR, NOAA/POES and the extreme ultraviolet (EUV) camera on board IMAGE. Charge-exchange losses, adiabatic drift mechanisms, and ring-current plasmasphere interaction are discussed as possible explanations for the unexpected local time behavior. Of these scenarios, a local time dependence of the PAD produced by the ring current-plasmaspshere interaction appears to be the more likely scenario although a combination with the other scenarios cannot be ruled out.

To fully analyze ENA data one needs to extract the parent ion distribution. There are several techniques to do this: One may use a forward modeling technique described and developed by *Roelof and Skinner* [2000]; or, one may use inversion techniques [*Twomey*, 1977] as has already been applied to IMAGE data by *Perez et al.* [2001]. However, one of the fundamental challenges of inverting ENA measurements arises from the fact that ionic plasma is emitting ENAs anisotropically according to its local PAD. This causes an ambiguity as to whether or not spatial variations in ENA ¤ux are due to spatial variations of the PADs or variations of the total ion ¤ux. The capability of the above mentioned techniques to resolve this pitch angle ambiguity is still uncertain, but progress is being made at the time of writing this paper. The pitch angle effect is signi£cant in the second event presented in this paper and we have choosen not to attempt to invert the ENA measurements. We instead use forward modeling to illustrate how different PADs can effect the ENA images.

The HENA instrument [*Mitchell et al.*, 2000] measures the direction of arrival and the velocity of ENAs. Although the instrument was designed to analyze the ENA mass with one of its two imaging systems, that system was not fully operational at the time of this event. Therefore, this paper discusses the ENA results under the assumption that hydrogen is the dominant species in the images. Independent examination of several storms suggests that this is a good assumption. The use of foils in HENA introduces a point spread in th eimages which ranges from 6°(at 50 keV) to 16°(at 16 keV) full width at half maximum.

2. 23 May 2000: Rapid dayside ion dropout

2.1. Observations

Plate 1a shows the IMF and below it in Plates 1b and 1c the ENA images observed by HENA at 16-50 keV (assuming that they are hydrogen). The IMF was measured by the WIND spacecraft with one minute resolution. At this time WIND was approximately 60 R_E upwind from the center of the Earth. The time has been corrected for the travel time from the point of measurement to the center of the Earth using the solar wind velocity measured from WIND. Lines are connected from the IMF plot to the times of observation of each ENA image. The ENA images in Plates 1b and 1c are presented in an azimuthal projection with a 120°×120°£eld of view (FOV). This projection is almost what a human eye

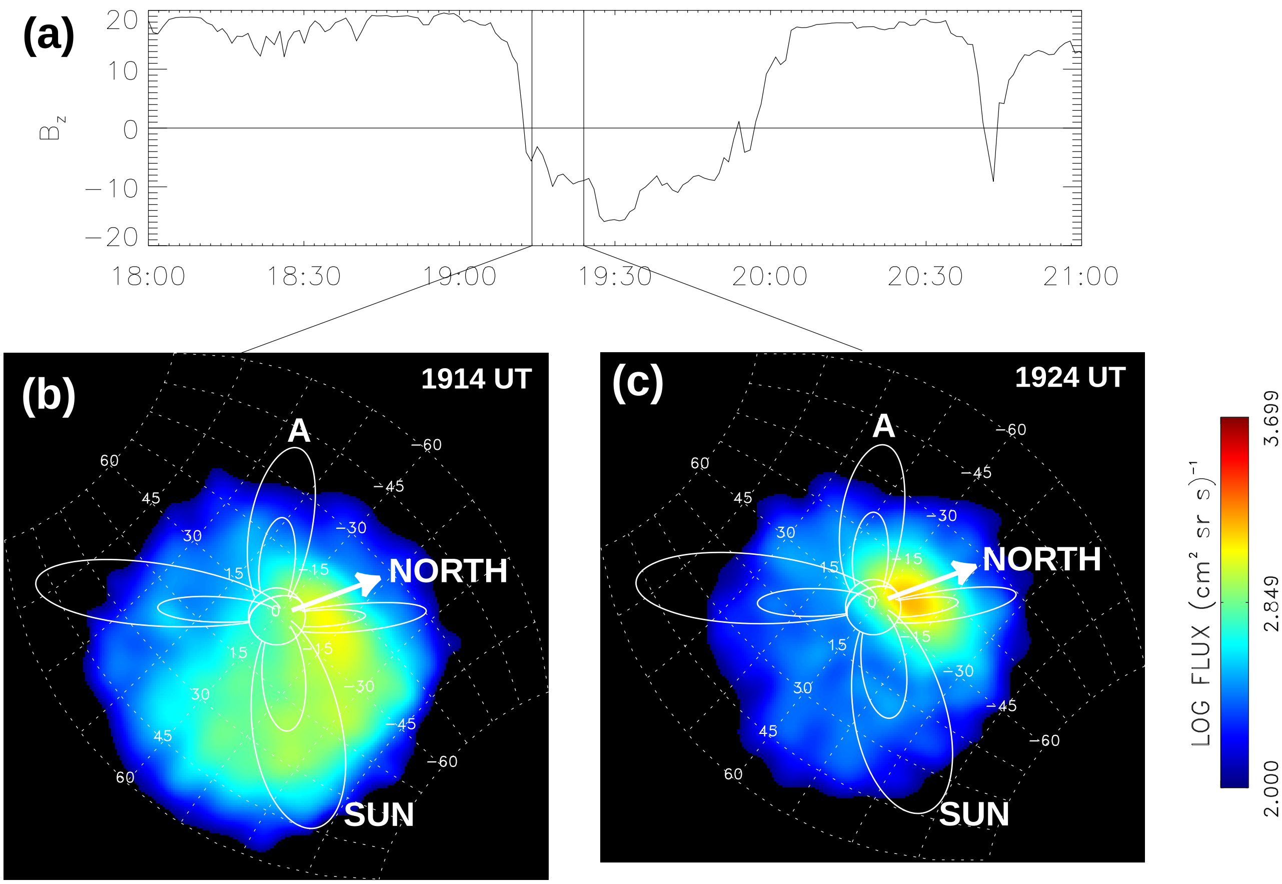

Plate 1. (a) The interplanetary magnetic £eld measured by WIND, (b) the observed ENA images (16-50 keV).

would see. To illustrate the projection one can think of the detector being located in the center of a sphere, with the pole of the sphere being the direction of the spin axis. The image has then been projected onto the surface of this sphere. The dashed gridlines in the background mark the latitude (horizontal lines) and the longitude (vertical lines) of this sphere. The latitude corresponds to the elevation angle in the instrument and the longitude corresponds to the spin angle. The coordinate system is geocentric. The circle about the center represents the limb of the Earth, while the arc inside the limb represents the terminator. The magnetic dipole £eld lines of L shells 4 and 8 are drawn for reference at noon, dawn, midnight, and dusk. The sunward pair of £eld lines are marked "SUN" and the "A" marks the antisunward (midnight) pair of £eld lines. The magnetic dipole vector is plotted approximately from the north pole. Both ENA images are taken from approximately 7.5 R_E altitude, 60° solar magnetic (SM) latitude, and -63° SM longitude.

The ENA image (1914 UT) in Plate 1b was taken when the maximum ENA ¤ux was observed on the dayside. Note that this is coincident with the rapid change to southward IMF. Before this time the ENA ¤ux had been increasing since around 1700 UT. After 1914 UT the ENA ¤ux starts decreasing and reaches background levels at 1924 UT, shown here in Plate 1c. At that point the ENA ¤uxes that appear to come from the noon meridian have decreased about a factor of 4. The fast timescales in this event immediately tells us that this cannot be an effect from changing vantage point or a change in PADs of the ions. The clear enhancement at the foot of the dusk £eld line is the intense ENA emissions coming from the nearly mirroring ions at about 300-400 km altitude. At this altitude the ions starts charge exchanging with the much more dense O and N_2 of the upper atmosphere [*Roelof*, 1997], which intensi£es the ENA ¤ux. The low altitude ENA emissions may come from the precipitating/mirroring ions from an injection on higher L shells on the nightside.

2.2. Model

We now trace protons with isotropic PAD in an attempt to explain the observations. Three simulated snapshots of the equatorial differential ¤ux of protons with 30° equatorial pitch angle at 30 keV are shown in Plates 2b-2d. From this particular vantage point of IMAGE, ENAs that originate from ions with 90°will not propagate towards the detector. Therefore we choose to show only the 30°protons since these are closer to the ions that the ENA images in Plate 1 actually capture. The protons are traced in a dipole magnetic £eld, a corotational electric £eld and the Volland-Stern type convection electric £eld [*Volland*, 1973; *Stern*, 1975] with a shielding factor of 1, whose electric potential Φ is expressed by

$$\Phi = \Phi_0 \frac{\sin\phi}{2} \left(\frac{R}{R_B}\right), \quad (1)$$

where Φ is the polar cap potential drop (PCP) in kV, Φ_0 is a coef£cient that depends on the IMF B_z and the clock angle of the IMF. The geocentric distance at a given point at the equator is denoted R and R_B is the geocentric distance of the magnetopause at 0600 MLT or 1800 MLT at the equator. R_B is given by

$$R_B = \frac{1}{\cos^2\lambda_{PC}} \text{ (Re)}, \quad (2)$$

where λ_{PC} is a latitude of the polar cap boundary. λ_{PC} is £xed to be 72° corresponding to R_B of 10.47 Re, which is consistent with statistical results of *Makita et al.* [1983]. The history of the PCP is obtained by the SuperDARN measurements [*Rhuohoniemi and Baker*, 1998] and is shown in Plate 2a. The source distribution function at L=10 is assumed to be isotropic Maxwellian with number density of 0.3 cm^{-3} and temperature of 5 keV. Details of the calculation are mentioned by *Ebihara et al.* [2001].

Plates 2b-2d show the snapshots of the modeled proton ¤ux at 1914, 1924, and 1944 UT on May 23, 2000. The modeled ¤ux has a maximum intensity at L=4-5 and the structure extends from midnight to the prenoon sector. After the sudden enhancement of the convection electric £eld at 1920 UT associated with the southward turning of IMF, the ¤ux near noon begins to decrease as shown in Plate 2c. Most of the intensities around noon are not signi£cantly diminished until 1944 UT (Plate 2d). The rapid decrease of the dayside ¤ux can be explained in terms of changes in drift trajectories of protons due to the enhancement of the large-scale convection electric £eld.

To simplify the comparison between model and observation we simulated ENA images using the ion distribution shown in Plates 2b-2d with an isotropic PAD and full loss cones. The simulated ENA images are shown in Plates 2e-2g. The vantage points are the same as for IMAGE. We see a that the dayside ion ¤uxes deacrease after the commencement of the convection electric £eld.

In order to illustrate the physical mechanism repsonsible for the decrease we show in Figure 1 the drift trajectories of protons with energy of 30 keV and equatorial pitch angle of 30° at L=5 (corresponding to 5.25 keV and 25° at L=10). We choose to show the 30°particles since this is the approximate pitch angle the line of sight (LOS) toward the noon emission region makes as it crosses the equatorial plane. Left panel of Figure 1 shows the trajectories for the case that the PCP is kept at 20 kV. The protons coming from

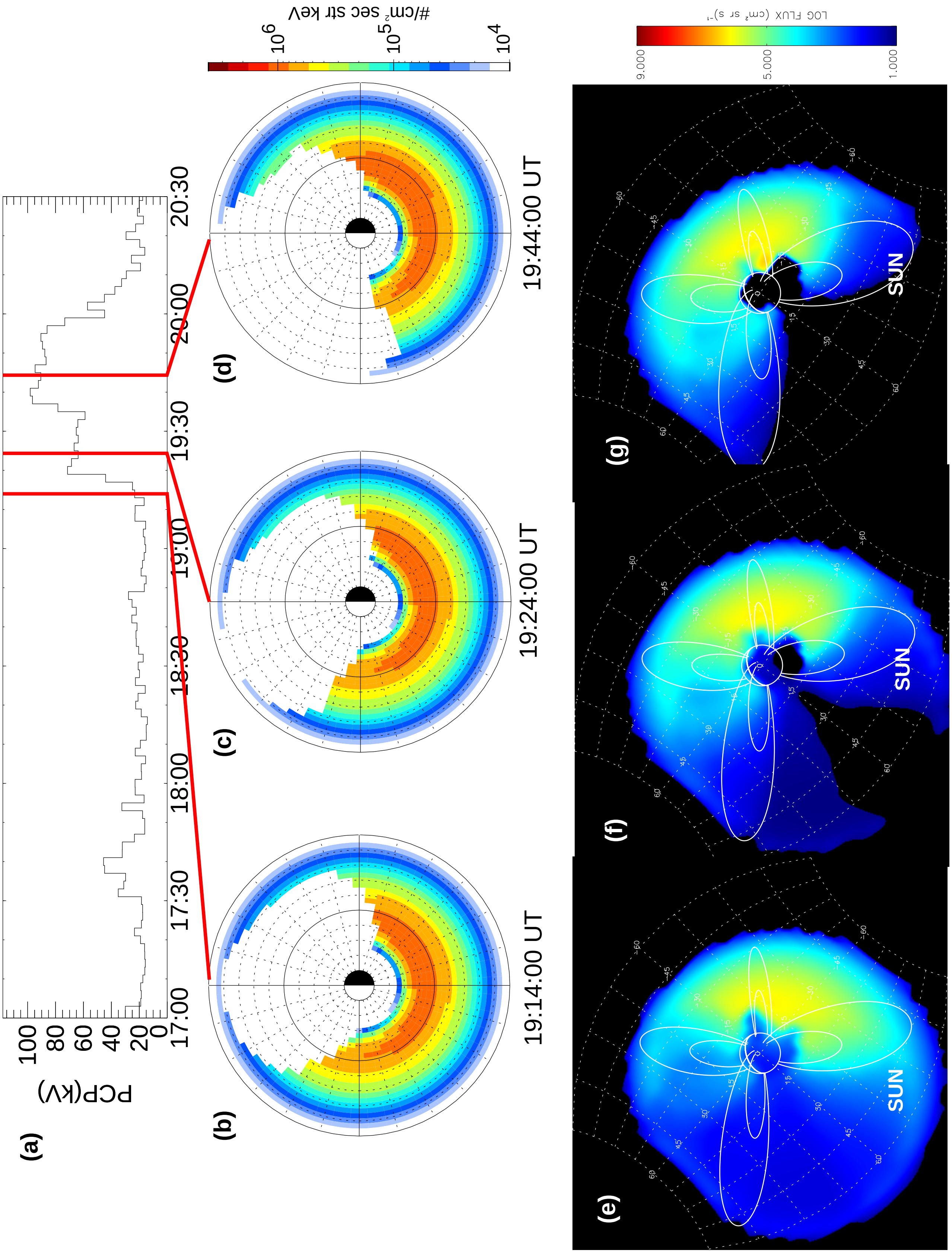

Plate 2. (a) The cross polar cap potential measured by Superdarn.(b)-(d) Snapshots of the 30° equatorial ion intensities at 30 keV from the model by *Ebihara and Ejiri* [2000]. (e)-(g) Simulated ENA images using the ion distribution above with isotropic pitch angle distribution.

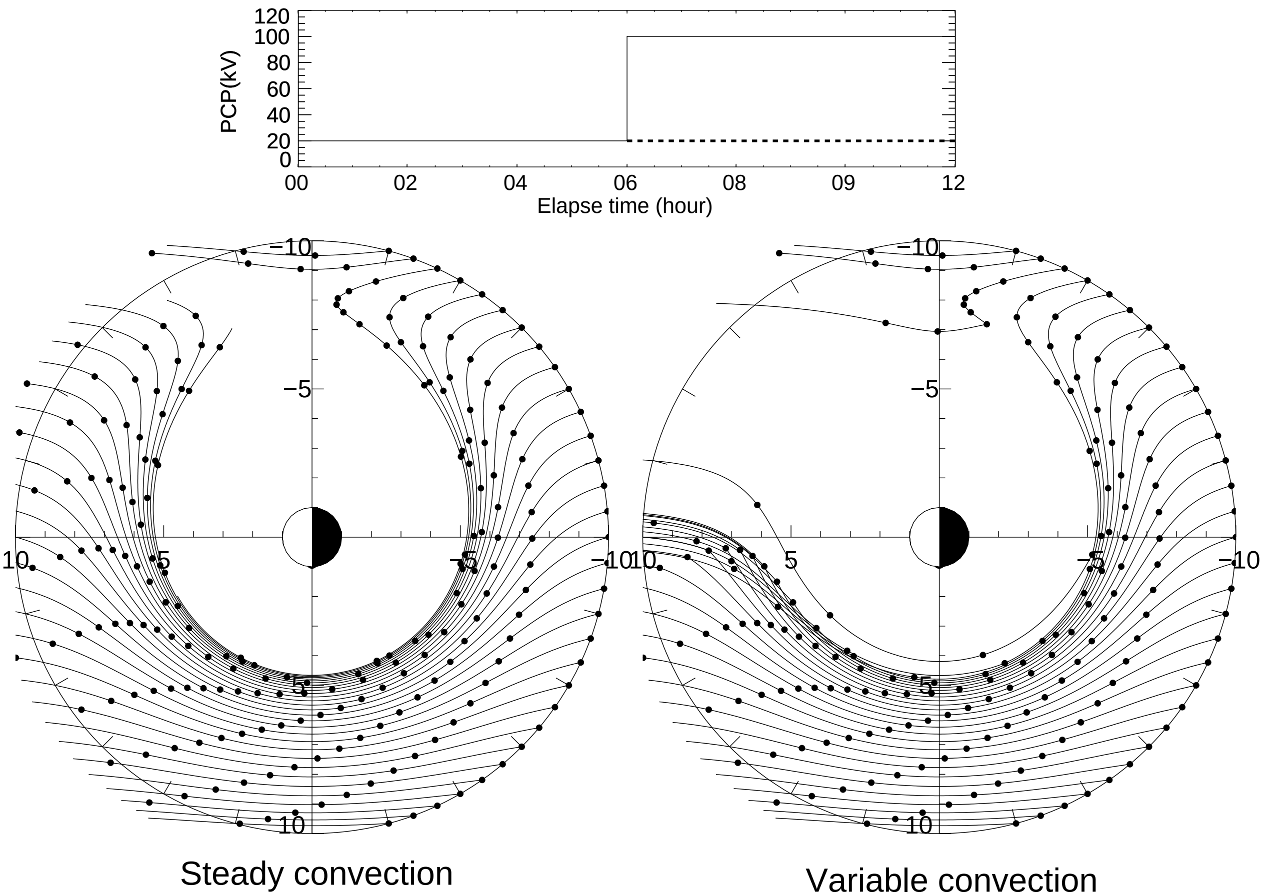

Figure 1. Drift trajectories of protons with magnetic moment of 0.030 keV/nT (equatorial pitch angle of 30° (25°) and energy of 30 (5.3) keV at L=5 (10)). Left panel shows the trajectories in the steady PCP of 20 kV. Right panel the trajectories in the variable convection electric £eld, that is, the PCP increases from 20 kV to 100 kV at the elapse time of 6 hours. The history of PCP used in the calculation is shown in the top panel.

the midnight-morning sector drift and escape from the noon-morning sector. If we increase the PCP at an elapsed time of 6 hours (right panel of Figure 1), a prominent change in the drift trajectories is found in the dayside region: They escape from the inner region rapidly in response to the enhancement of the PCP. As a consequence, the proton ¤ux near noon and the prenoon region is expected to drop out rapidly. This tendency is in agreement with the IMAGE observation shown in Plate 1. However, two discrepancies between the observation and the simulation are found. First, the observed ¤ux in the evening sector decreases in response to the PCP enhancement whereas the simulation displays only a decrease in the noon sector. This discrepancy may come from the the fact that the obtained spatial ¤ux distribution depends on the initial distribution of the ions. In the calculation, the initial distribution is kept constant. More realistic initial distribution would be needed to examine the changes in the spatial distribution of the ¤ux. Second, and more important, the observed ¤ux decreases much more rapidly (with a time scale of $\sim$10 minutes) than the simulated. *Ridley et al.* [1998] and *Shepherd et al.* [1999] have shown that the dayside ionosphere can respond within minutes to changes in IMF which is consistent with our results here. Also, *Liemohn et al.* [2001] obtained realistic results in modeling the storm-time ring current assuming that the PCP and the inner magnetospheric convection pattern vary as rapidly as the high-latitude ionosphere varies with IMF, using the assimilative mapping of ionospheric electrodynamics (AMIE) inversion technique to compute the PCP. In conclusion we can say that the ring current changes its con£guration within a few minutes from where the IMF B_z goes negative. In general, the ENA ¤ux could change due to a change in PAD (see below). However, we £nd it dif£cult to justify that PADs can change during only 10 min. Moderate to strong pitch angle diffusion usually has time scales of hours and not minutes. Also pitch angle diffusion would lead to precipitation of the ions which would produce an ENA signal from low altitude. This is not observed. That leaves an evacuation of the ion distribution through the dayside magnetopause as the most realistic explanation.

3. 24 May 2000: Ring current - plasmasphere interaction?

3.1. Storm conditions

The 24 May storm was relatively stable in terms of IMF and magnetospheric convection. The three components of the IMF are shown in Figure 2. For later reference the times corresponding to the times of the ENA images in Plate 3 are shown as solid, vertical lines. The dotted vertical line at 0250 UT is the time of maximum precipitation on the duskside as observed by the NOAA/POES satellite, which will be shown below in Plate 6. The dashed lines at 0906 UT, 1120 UT, 0320 UT and 0606 UT are the times of the Polar in-situ measurements that will be shown below in Figure 4. Around 0250 UT on 24 May the IMF-B_z went down to approximately -30 nT for a couple of hours. This caused an enhanced convection £eld in the magnetosphere that brought plasma to low L-shells. The IMF reverted to a more normal magnitude after approximately 1700 UT on 24 May. The IMF B_z stayed around -5 nT from this point until approximately 1700 UT on 26 May. The D_{st} index for this storm is shown in Figure 3.

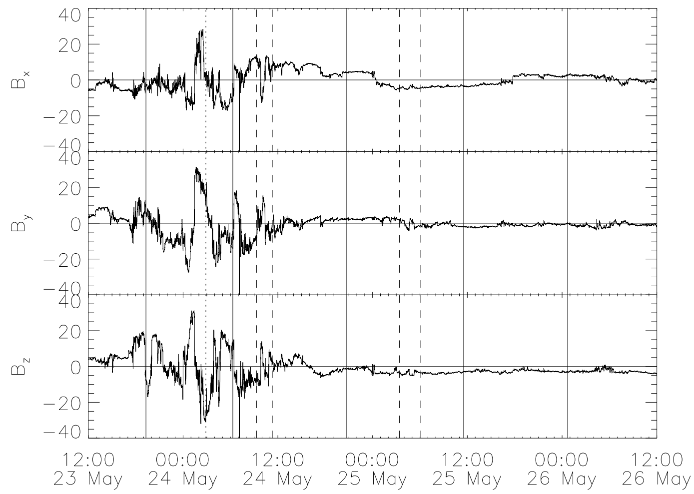

Figure 2. The interplanetary magnetic £eld. Vertical solid lines are the times of ENA observations. The vertical dotted line is the time of maximum precipitation as seen by the NOAA/POES satellite on the duskside and shown in Plate 6. The dashed lines are the times of in-situ measurement by Polar in Figure 4.

3.2. ENA and EUV observations

Plate 3 shows four pairs of ENA images in two energy ranges taken when IMAGE passed approximately above the north pole. The £rst column is taken at 24 May 0618 UT, approximately in the mainphase, the second is taken at 24 May 2040 UT, the third at 25 May 1132 UT, and the fourth 26 May 0042 UT. The £rst and second rows in Plate 3 covers 16-27 keV and 39-60 keV, respectively. All images in Plate 3 are presented in the same format as for Plate 1. The solid contours display the pitch angle that the LOS to each pixel makes as it crosses the equatorial plane. We see that for the visible ring current, HENA views equatorial pitch angles less than approximately 40°below L=4. In the bottom row (Plate 3e-3h) we have overlayed the traces of the sharp gra-

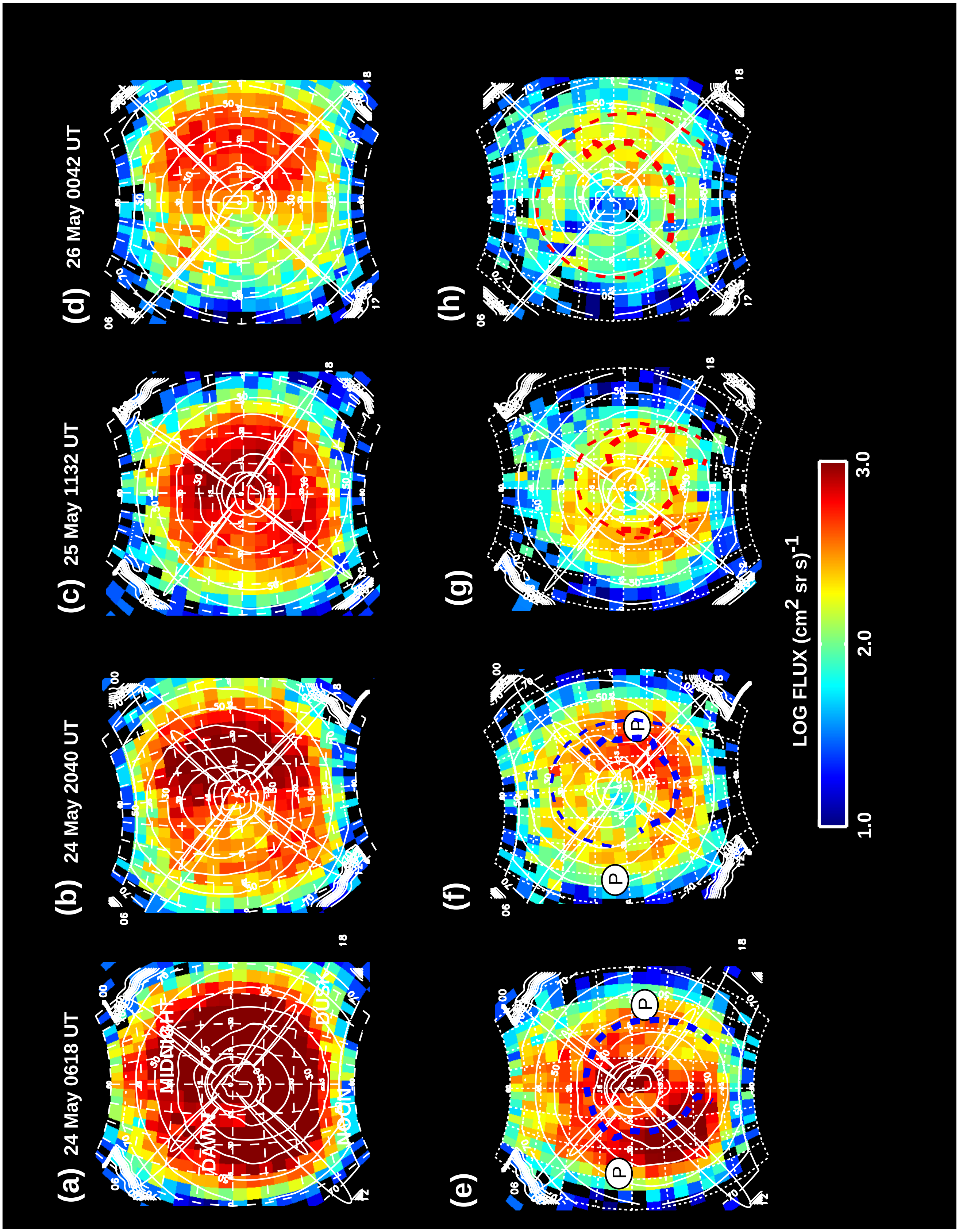

Plate 3. ENA images taken from approximately above the north pole. Energy goes down and time goes left to right. Images are taken about 14 hours apart. (a)-(d) 16-27 keV, (e)-(h) 39-60 keV. Noon is the lower left £eld line in each image and the approximate equatorial position of Polar (see Figure 4) is marked with a “P”.

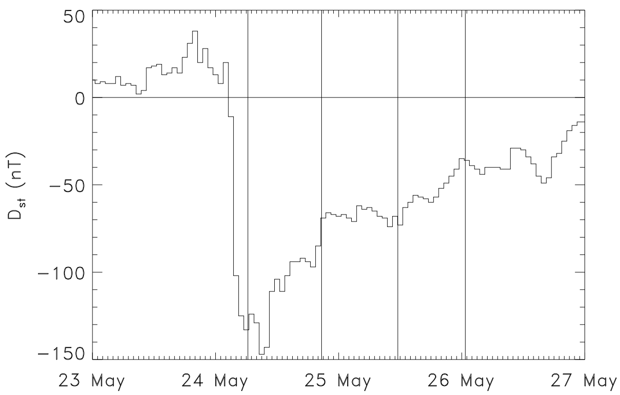

Figure 3. The D_{st} index. Times of the ENA observations are indicated by vertical lines.

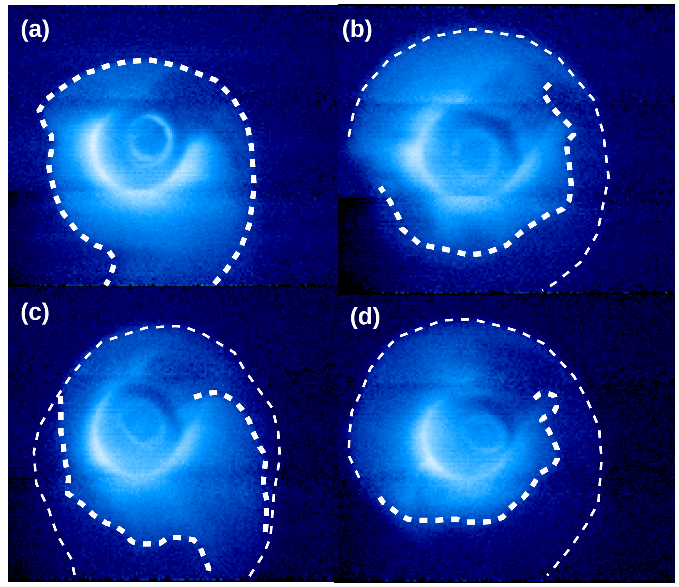

Plate 4. EUV images from the same times as for the columns of Plate 3. Dashed contours mark the gradients in the emission rate found. Thin dashed lines mark that a more diffuse gradient was found and bold, dashed lines mark that a sharp gradient was found.

dients in the plasmasphere observed simultaneously by the EUV camera on board IMAGE. These traces are marked by dashed lines in contrasting colors blue and red. The approximate location of Polar is marked with “P” in Plates 3e-3f.

The £rst column (24 May 0618 UT) at 16-27 keV shows signi£cant ENA ¤uxes extending westward from midnight almost to dawn. However, for the higher energy channel (39-60 keV) the ENA ¤uxes coming from the duskside are almost one order of magnitude lower than the ENA ¤uxes coming from the dayside. The second column (24 May 2040 UT) shows ¤uxes around the dusk region for all energies. The third column (25 May 1132 UT) shows the same behavior as the £rst column, and the last column (26 May 0042 UT) displays the same pattern as the second column.

Note the apparent correlation between the lack of ENA ¤ux and the existence of a plasmaspheric tail [*Grebowsky*, 1970]. The plasmapause traces were obtained from the EUV images presented in Plate 4. The images were taken at the same time as the ENA images in Plate 3 by the EUV camera on board IMAGE [*Sandel et al.*, 2000]. The images are shown in a logarithmic scale; calibrated intensities are not yet available. The extended shadow in the upper right corner is the shadow of the Earth. Hence the sun is to the lower left in each image. The tracing algorithm analyzes a LOS de£ned by a selected pixel in the EUV image. It £nds the minimum value of L along the LOS, and reports the magnetic local time and magnetic longitude of the point of minimum L. This algorithm is an adequate approximation from polar vantage points but is not valid for near equatorial vantage points. The more general algorithm by *Roelof and Skinner* [2000] has not yet been implemented. In most cases, we found two gradients: one sharp, marked with a bold dashed line, and one more diffuse gradient marked with a thin dashed line.

3.3. Polar proton observations

In order to investigate the apparent relation between the plasmaspheric tail and the lack of ENA ¤uxes we show in-situ measurements by the imaging proton spectrometer (IPS) on board the Polar spacecraft in Figure 4.

Two energies are shown, 18.9 and 43.1 keV, for four different positions as marked. Figure 4a and 4b are obtained at the duskside and morningside 3 and 5 hours after the time of the £rst column of Plate 3. Likewise, Figure 4c and 4d are obtained on the duskside and morningside 6 and 9 hours after the time of the second column of Plate 3.

The two £rst measurements in Figures 4a and 4b are obtained on approximately the same L-shell on the morning of 24 May, but at different MLT and magnetic latitude. Although Figure 4a displays only a limited pitch angle range (due to the high latitude) the PADs on the duskside have a sharp increase around 20°. Note also that the PADs shown in Figures 4a and 4d appear to be more isotropic at the lower energy. The LOS from HENA towards the equatorial point where Polar obtained the duskside measurement in Figure 4a cuts the equatorial plane at approximately 40°pitch angle. Similarly this angle is approximately 50°for the dawnside measurement of Polar shown in Plate 3e. Then according

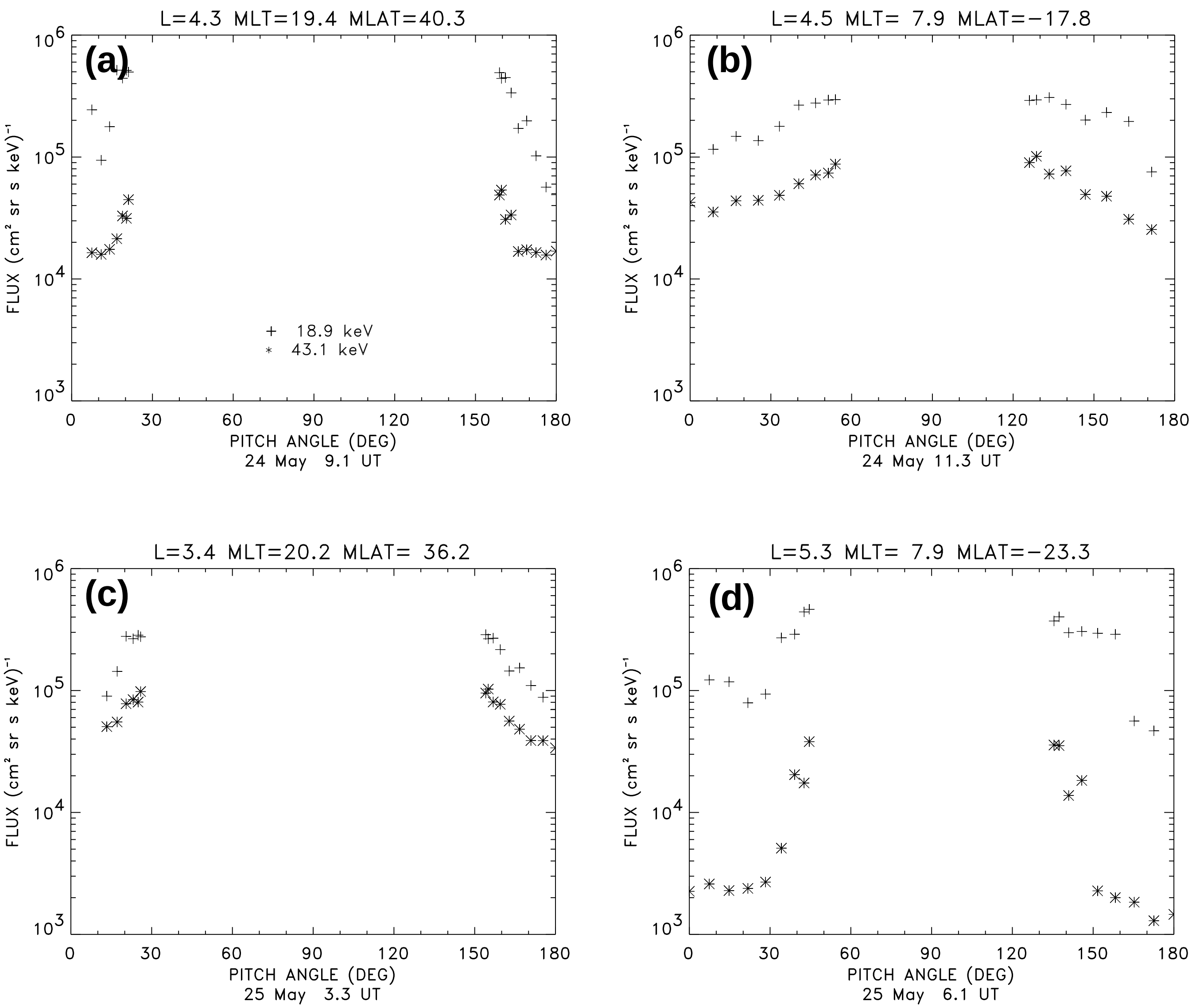

Figure 4. Pitch angle distributions (PAD) mapped to the equator obtained by the imaging proton spectrometer onboard Polar. (a) Duskside for the 24 May 0906 UT at L=4.3. (b) Dawnside for the 24 May 1120 UT at L=4.5. (c) Duskside for the 25 May 0330 UT at L=3.4, and (d) dawnside for the 25 May 0606 UT at L=5.3. Note that PADs are more peaked around 90°on the duskside for the 24 May and more peaked on the dawn side for the 25 May.

to Figures 4a and 4b the ENA ¤ux coming from the equator towards HENA in the 40°pitch angle direction would be as high as that coming from the dawnside in Plate 3e. This is in agreement with the ENA ¤ux seen at the two observation points of Polar in Plate 3e.

Figures 4c and 4d show the PADs obtained from Polar on somewhat different L-shells as indicated in the £gure. Now it appears that the general shape of the PADs on the duskside in Figure 4a has somehow been transferred to the morningside. In summary, the PADs depend on both MLT, time and energy in a manner consistent with the ENA images shown in Plate 3.

In order to illustrate the effect on ENA images due to local time dependent PADs, we have modeled the equatorial ion distribution using the parametric model developed by *Roelof and Skinner* [2000]. This model uses 38 parameters to express the shape and PADs of the equatorial distribution. The azimuthal dependence is a second order harmonic expansion using £ve parameters. The L-shell dependence is expressed through gaussian functions using 6 parameters. The PAD uses two parameters based on squared sine and cosine functions. Each of the L parameters and those for the PADs are then expanded into £rst and second order harmonics in azimuth. The ENA ¤ux for each pixel is then calculated by integrating the ion distribution, charge exchange cross section and the chamberlain hydrogen geocorona [*Chamberlain*, 1963; *Rairden et al.*, 1986] over the LOS. The instrumental response function is then convoluted over the image pixels to produce the ENA image. The satellite vantage point is similar to the ones for the images in Plate 3. The simulated ENA image is displayed in Plate 5a with the noon £eld lines to the lower left. Although this example is only illustrative we have aimed to match the ion distributions to the observed ENA image in Plate 3e. For the dayside we have used a PAD similar to the one found in Figure 4b and for the nightside we have used a PAD similar to the one in Figure 4a. This example shows that it is possible to explain the local time variations in the ENA observations in terms of local time dependent PADs.

4. Discussion

In the 23 May event we saw two discrepancies between the modeled ion distributions and the observed. First, the observed ENA images implied that the ion distribution before the rapid decrease was closer to the Earth than the model suggests. Second, the evacuation of the ion distribution appeared much faster than could be reproduced by the model. This may imply that the recon£guration of drift trajectories was more dramatic than the recon£guration of the model trajectories in Figure 1. If, for example, the ion drift trajectories at L=5 would go out through the dusk-afternoon magnetopause, instead of noon, after the southward turning of the IMF. This may account for a more rapid evacuation of the dayside ion distribution.

In the 24 May observations it is a question what could cause the apparent relation between the plasmaspheric tail and the lack of ENA ¤ux. Based on the PAD measurements by Polar it is tempting to suggest that the plasmaspheric tail interacted with the ring current ions and modi£ed their PADs.

It is known that pitch angle diffusion can be triggered by an interaction between the ring current and the plasmasphere through EMIC wave resonance[*Jordanova et al.*, 1997]. This interaction diffuses particles below a certain pitch angle into the loss cone. The result is a PAD with low and isotropic ¤uxes below a certain pitch angle that is determined by the resonance condition for the EMIC wave resonance. Above the speci£c pitch angle the PADs are essentially unaffected, which leaves us with a “hat-like” distribution that may be interpreted as more “rounded” PAD than before the interaction. This behavior has been observed during storms by *Willams and Lyons* [1974] and *Joselyn and Lyons* [1976]. This scenario is further supported by observations of proton precipitation by the total energy detector (TED) on board the NOAA-15 POES satellite which orbits the Earth in 105 min. The TED detects precipitating protons in the energy range 0.05-20.0 keV. Plate 6 shows the differential energy ¤ux of precipitating protons. The data has been sorted into time and L-shell bins and sampled from the 1500-2100 MLT region. Note the signi£cant precipitation down to L=2 in the beginning of the storm and lasting approximately 5 hours. The characteristic energy of these protons is about 10 keV. Data on the dawnside showed no precipitation on low L shells during this time. The white horizontal lines show the times of ENA observations shown in Plate 3. This type of precipitation has been associated with pitch angle diffusion into the atmospheric loss cone driven electromagnetic ion cyclotron (EMIC) wave-particle interactions as reported by e.g. *Cornwall et al.* [1971] and *Hultqvist et al.* [1976].

Charge exchange is also known to produce more rounded PADs in the ring current, since ions with smaller pitch angles reach lower altitudes where the neutral density is higher. However, the charge exchange cross section decreases with energy, so that the roundness of the PADs from charge exchange is expected to decrease with increasing energy, and not increase as observed.

PADs can also become more peaked around 90°as the ions drift adiabatically in to a region with higher magnetic £eld strength during which their perpendicular energy will increase [*Ejiri*, 1978; *Chen et al.*, 1999]. By assuming a cer-

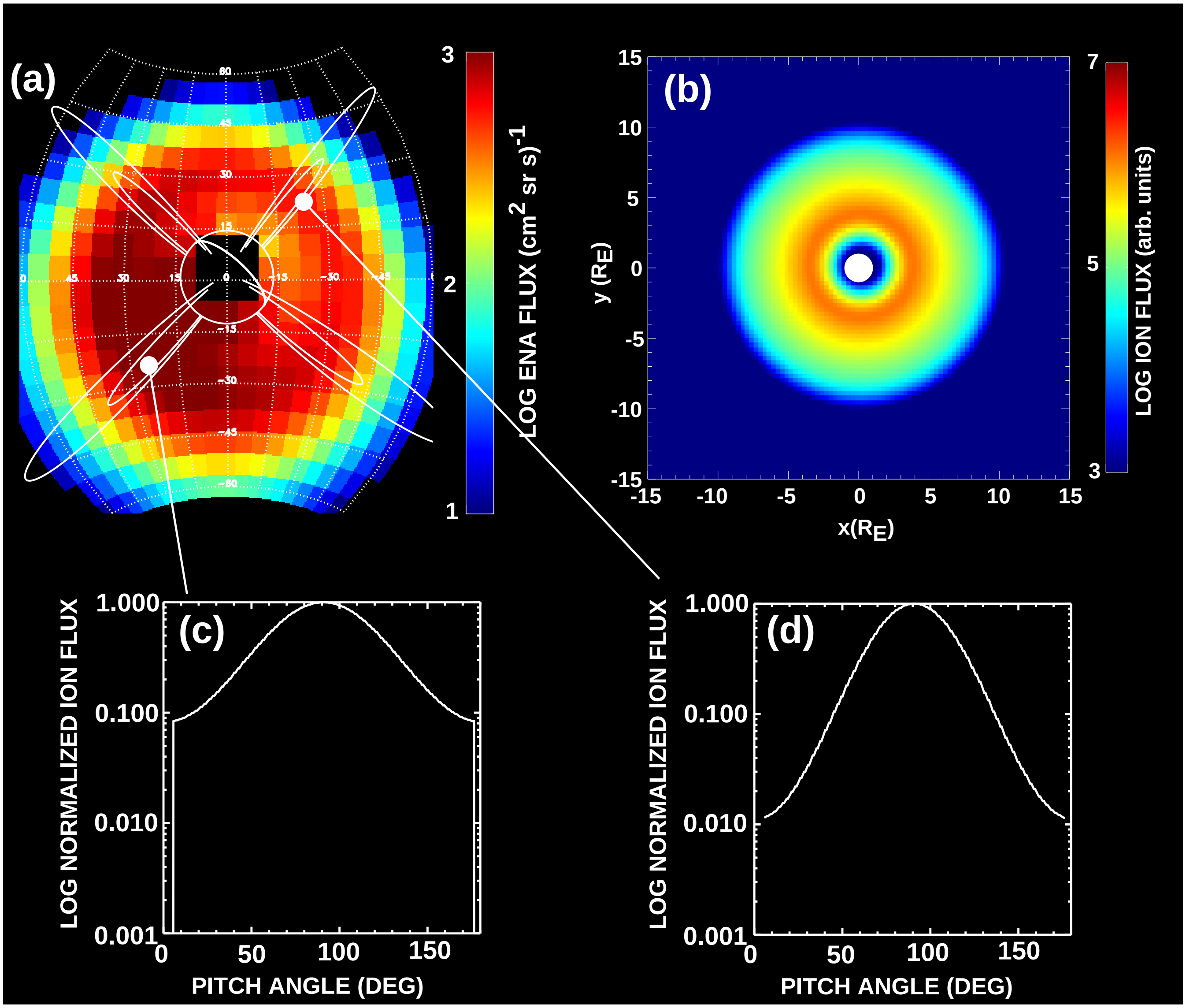

Plate 5. (a) Simulated ENA image for 39-60 keV based on the HENA observations on 24 May 0618 UT shown in Plate 3e. (b) The equatorial proton distribution used to simulate the ENA image. Protons with 90°are shown. Note that the distribution is azimuthally symmetric for this pitch angle. (c) The dayside PAD used in the model and (d) the nightside PAD used in the model.

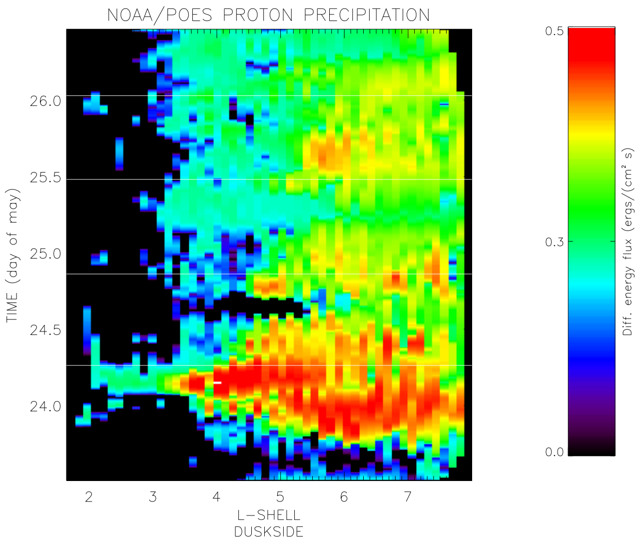

Plate 6. Proton precipitation measured in differential energy ¤ux detected by the NOAA/POES satellites. The horizontal white lines mark the times of observations in Plate 3. Strong precipitation for L$<$4 can be seen early in the beginning of the storm when hot plasma is injected onto low shells.

tain shape of the initial energy spectrum, one may be able to account for the observed increasing roundness of the PADs with increasing energy. However, it is dif£cult to explain the local time behavior of the observed PADs.

Figure 5 illustrates a possible scenario for the ring current-plasmasphere interaction. Ions drift in from the plasma sheet (Figure 5a) to the inner magnetosphere where the PADs become more peaked around 90°pitch angle through conservation of the £rst adiabatic invariant (Figure 5b). When a plasmaspheric tail is suddenly formed, EMIC waves may resonate with the ring current ions and drive ions below a certain pitch angle (as determined by the local resonance condition) towards the loss cone. This would produce a more hat-like PAD as shown in Figure 5c. During this process, heavy precipitation is observed by low-altitude spacecraft as shown in Figure 5d and Plate 6. The ions on the dayside have not been effected by the tail (Figure 5e).

5. Summary and conclusions

We have presented the initial analysis of ENA images from the ENA imager HENA onboard the IMAGE satellite. Two examples of unexpected events were investigated in this paper: (1) A rapid decrease of the dayside ion ¤uxes during only 10 min on the 23 May, 2000; (2) The development of the storm on the 24 May, 2000 where the ring current displayed an unexpected local time distribution closely related to the shape of the plasmasphere.

In the £rst event the ENA ¤uxes of the dayside ring current were observed to build up from around 1700 UT to 1914 UT on 23 May, 2000. The IMF B_z during this period reached about +20 nT. Then, the ENA ¤uxes suddenly decreased for about 10 min until they reached a constant value which was about 4 times less than the maximum ¤uxes observed. The decrease of the ENA ¤uxes started (to within a few minutes accuracy) when the IMF B_z went negative. Using the ring current model by *Ebihara and Ejiri* [1999] we could conclude that the rapid decrease of the dayside ring current ¤uxes was due to a rapid change of the drift trajectories to a more open con£guration. The observed decrease of the dayside ¤ux took place in 10 min whereas the modeled ring current took about 30 min to recon£gure itself. Our conclusions from the £rst event are as follows.

1. The ion drift paths of the inner magnetosphere are strongly dependent on solar wind IMF B_z for ions of energy 16-50 keV.

2. The resulting induced, convectional electrical £eld penetrates the dayside inner magnetosphere within a couple of minutes of the southward turning of the IMF.

3. After southward turning of the IMF the ring current ¤uxes decrease due to convection out through the magnetopause.

In the second event, ENA images of the ring current and EUV images of the plasmasphere from above the north pole during the storm of the 24 May, 2000, revealed lower ENA ¤uxes where a plasmaspheric tail was present. In-situ data from Polar suggested that the change in ENA ¤ux could be due to a variation of PADs with local time. We suggested the possibility that this change in PAD was an effect of pitch angle diffusion triggered by the interaction between the hot ions in the ring current and the electrons in the plasmasphere. Unlike the £rst event, the observed time scales in the second event were long enough to permit evolution of the PADs through pitch angle diffusion.

This study have illustrated two opposing aspects of ENA measurements. One where the dynamics in the ENA images were due to variations in the ion ¤ux, and one that were due to the variation of the PAD of the ion distribution. These aspects produces an ambiguity in the analysis of ENA measurements that has to be adressed through supporting in-situ measurements and physical reasoning.

Future studies will consist of closer comparison with ring current modeling including wave-particle interaction with realistic plasmasphere models such as the ones by *Fok et al.* [1996] and *Kozyra et al.* [1997]. It may also be of interest

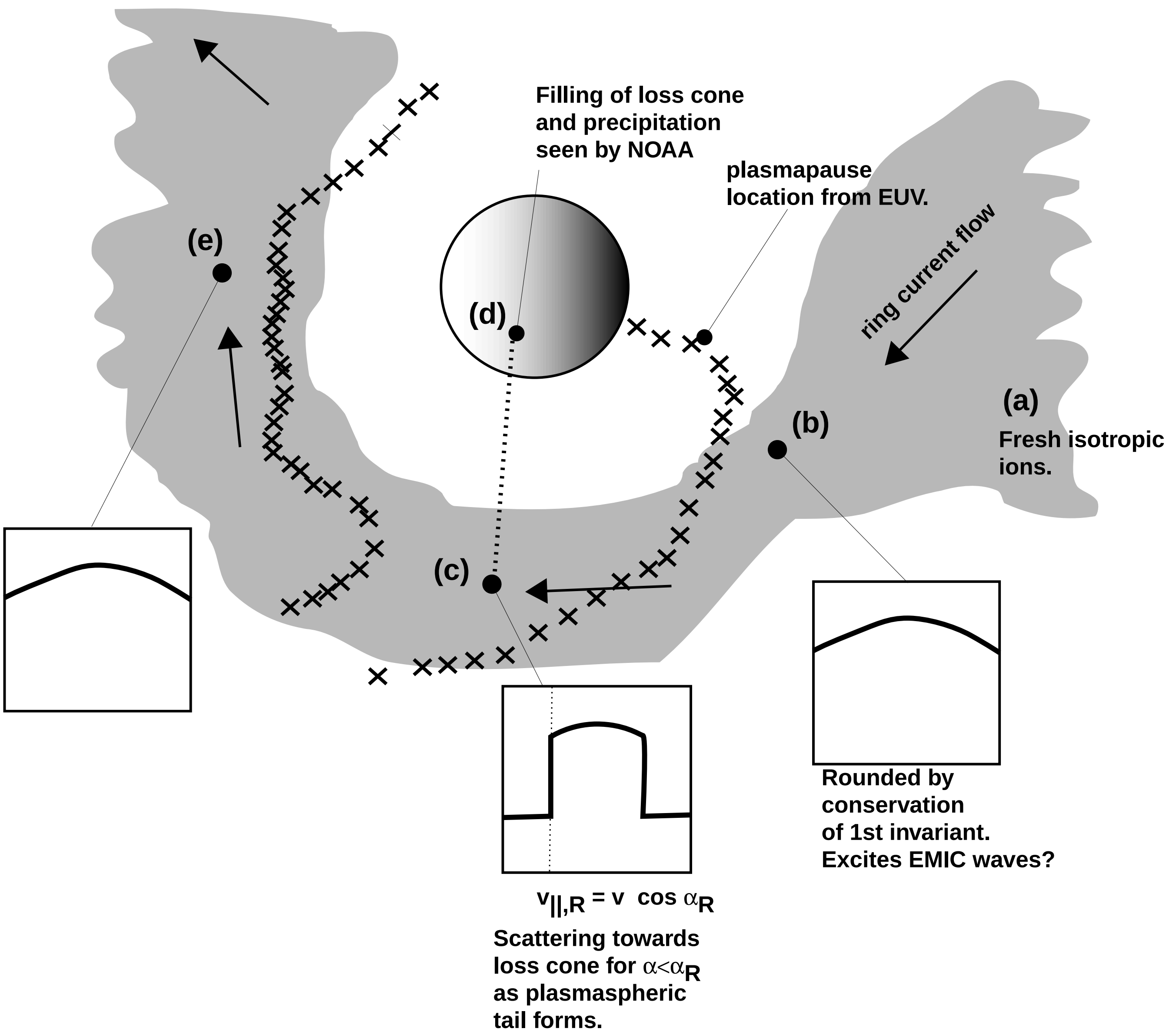

Figure 5. Sketch illustrating a possible scenario for the ring current-plasmasphere interaction. View is from above the north pole and the sun is to the left.

to investigate the EMIC wave activity on this date, as well as the distribution of ions in the loss cone from low altitude spacecraft.

Acknowledgments. The authors like to thank the WIND magnetometer data processing team in the NASA/GSFC Laboratory for Extraterrestrial Physics and Dr. S. Shepherd at Applied Physics Laboratory, Maryland, for processing the Superdarn data. We would also like to thank D. Evans for kindly providing NOAA/POES data, M. Henderson and especially R. Friedel at Los Alamos National Laboratories for processing the POLAR/IPS pitch angle data. Thanks to M. Schulz at the Lockheed Martin Advanced Technology Center in Palo Alto, CA for fruitful discussions, and to the ACE SWEPAM and Dr. N. Ness at the ACE Science Center for providing solar wind data. Special thanks to Dr. M. Liemohn at University of Michigan for helpful discussions.

References

Barabash, S., Satellite observations of the plasma-neutral coupling near Mars and the Earth, Ph.D. thesis, Swed. Inst. of Space Phys., Kiruna, 1995.

Burch, J. L., ed., *The IMAGE mission*, Kluwer Academic, 2000, reprinted from *Space Sci. Rev.*, vol. 91, Nos. 1-2, 2000.

Chamberlain, J. W., Planetary coronae and atmospheric evaporation, *Planetary and Space Sci.*, pp. 901–960, 1963.

Chen, M. W., J. L. Roeder, J. Fennell, L. R. Lyons, R. L. Lambour, and M. Schulz, Proton ring current pitch angle distributions: Comparison of simulations with CRRES observations, *J. Geophys. Res.*, , *104*, 17,379–17,389, 1999.

Cornwall, J. M., F. V. Coroniti, and R. M. Thorne, Turbulent loss of ring current ions, *J. Geophys. Res.*, , *75*, 4699–4709, 1970.

Cornwall, J. M., H. H. Hilton, and P. F. Mizera, Observations of precipitating protons in the energy range 2.5 kev $\leq$ e $\leq$ 200 kev, *J. Geophys. Res.*, , *76*, 5220, 1971.

C:son Brandt, P., S. Barabash, O. Norberg, R. Lundin, E. C. Roelof, and C. J. Chase, ENA imaging at low altitudes from the Swedish micro satellite Astrid: Images and spectral analysis, *J. Geophys. Res.*, *104*, 2367–2379, 1999.

Ebihara, Y., and M. Ejiri, Quantitative ring current model: overview and comparison with observations, *Adv. polar Upper Atmos. Res.*, pp. 1–36, 1999.

Ebihara, Y., and M. Ejiri, Simulation study on the fundamental property of the storm-time ring current, *J. Geophys. Res.*, , *105*, 15,843, 2000.

Ebihara, Y., M. Yamauchi, H. Nilsson, R. Lundin, and M. Ejiri, Wedge-like dispersion of sub-kev ions in the dayside magnetosphere: Particle simulation and viking observation, *J. Geophys. Res.*, *, in press*, 2001.

Ejiri, M., trajectory traces of charged particles in the magnetosphere, *J. Geophys. Res.*, *83*, 4798–4810, 1978.

Fok, M. C., T. E. Moore, and M. E. Greenspan, Ring current development during storm main phase, *J. Geophys. Res.*, , *101*, 15,311–15,322, 1996.

Grebowsky, J. M., Model study of plasmapause motion, *J. Geophys. Res.*, , *75*, 4329–4333, 1970.

Henderson, M. G., G. D. Reeves, H. E. Spence, R. B. Sheldon, A. M. Jorgensen, J. B. Blake, and J. F. Fennell, First energetic neutral atom images from polar, *Geophys. Res. Lett.*, *24*, 1167–1170, 1997.

Hultqvist, B., W. Riedler, and H. Borg, Ring current protons in the upper atmosphere within the plasmasphere, *Planetary and Space Sci.*, *24*, 783, 1976.

Jordanova, V. K., J. U. Kozyra, A. F. Nagy, and G. V. Khazanov, Kinetic model of the ring current atmosphere interactions, *J. Geophys. Res.*, , *102*, 14,279–14,291, 1997.

Joselyn, J. A., and L. R. Lyons, Ion cyclotron wave growth calculated from satellite observations of the proton ring current during storm recovery, *J. Geophys. Res.*, , *81*, 2275–2282, 1976.

Kozyra, J. U., V. K. Jordanova, R. B. Horne, and R. M. Thorne, Modeling of the contribution of electromagnetic ion cyclotron (EMIC) waves to stormtime ring current erosion, in *Magnetic storms*, Geophysical monograph 98, American Geophysical Union, 1997.

Liemohn, M. W., J. U. Kozyra, M. F. Thomsen, J. L. Roeder, G. Lu, J. E. Borovsky, and T. E. Cayton, The dominant role of the asymmetric ring current in producing the stormtime dst, *J. Geophys. Res.*, 2001, in press.

Makita, K., C. I. Meng, and S. I. Akasofu, The shift of the auroral electron precipitation boundaries in the dawn-dusk sector in association with geomagnetic activity and interplanetary magnetic £eld, *J. Geophys. Res.*, , *88*, 7967–7981, 1983.

Mitchell, D. G., et al., *The imaging neutral camera for the Cassini mission to Saturn and Titan*, vol. 103 of *Geophysical Monograph*, AGU, Washington, DC, 1998.

Mitchell, D. G., et al., High energy neutral atom (HENA) imager for the IMAGE mission, *Space Sci. Rev.*, *91*, 67–112, 2000.

Perez, J. D., G. Kozlowski, P. C. Brandt, D. G. MItchell, J. M. Jahn, C. J. Pollock, and X. Zhang, Initial ion equatorial pitch angle distributions from energetic netural atom images obtained by IMAGE, *Geophys. Res. Lett.*, 2001, in press.

Rairden, R. L., L. A. Frank, and J. D. Craven, Geocoronal imaging with dynamics explorer, *J. Geophys. Res.*, *91*, 13,613–13,630, 1986.

Rhuohoniemi, J. M., and K. B. Baker, Large-scale imaging of high-latitude convection with super dual auroral radar network hf radar observations, *J. Geophys. Res.*, *103*, 20,797–20,811, 1998.

Ridley, A. J., G. Lu, C. R. Clauer, and V. O. Papitashvili, A statistical study of the ionospheric convection response to chaning interplanetary magnetic £eld conditions using the assimilative mapping of ionospheric electrodynamics technique, *J. Geophys. Res.*, , *103*, 4023–4039, 1998.

Roelof, E. C., Energetic neutral atom image of a storm-time ring current, *Geophys. Res. Lett.*, *14*, 652–655, 1987.

Roelof, E. C., ENA emissions from nearly mirroring magnetospheric ions interacting with the exobase, *Adv. Space Res.*, *20, (3)*, 361–366, 1997.

Roelof, E. C., and A. J. Skinner, Extraction of ion distributions from magnetospheric ENA and EUV images, *Space Sci. Rev.*, *91*, 437–459, 2000.

Roelof, E. C., D. G. Mitchell, and D. J. Williams, Energetic neutral atoms (E≈50 keV) from the ring current: IMP 7/8 and ISEE 1, *J. Geophys. Res.*, *90*, 10,991–11,008, 1985.

Sandel, B. R., et al., The extreme ultraviolet imager investigation for the IMAGE mission, *Space Sci. Rev., 91, (1/2)*, 197–242, 2000.

Sergeev, V. A., E. M. Sazhina, N. A. Tsyganenko, J. Å, Lundblad, and F. Søraas, Pitch-angle scattering of energetic protons in the magnetotail current sheet as the dominant source of their isotropic precipitation into the nightside ionosphere, *Planetary and Space Sci.*, *31*, 1147–1155, 1983.

Shepherd, S. G., R. A. Greenwald, and J. M. Ruohoniemi, A possible explanation for rapid, large-scale ionospheric responses to southward turnings of the imf, *Geophys. Res. Lett.*, , *26*, 3197–3200, 1999.

Stern, D. P., The motion of a proton in the equatorial magnetosphere, *J. Geophys. Res.*, *80*, 595, 1975.

Twomey, S., *Introduction to the mathematics in remote sensing and indirect measurements*, Developments in geomathematics 3, 1st ed., Elsevier scienti£c publishing company, 1977.

Volland, H., A semiempirical model of large-scale magnetospheric electric £elds, *J. Geophys. Res.*, *78*, 171, 1973.

Willams, D. J., and L. R. Lyons, The proton ring current and its interaction with the plasmapause: Storm recovery phase, *J. Geophys. Res.*, *79*, 4195–4207, 1974.

Pontus C:son Brandt, The Johns Hopkins University, Applied Physics Laboratory, 11100 Johns Hopkins Rd., Laurel, MD 20723-6099, USA

This preprint was prepared with AGU's LaTeX macros v4, with the extension package 'AGU^{++}' by P. W. Daly, version 1.6b from 1999/08/19.